Matter and Radiation at Extremes REVIEW scitation.org/journal/mre

Chemistry under extreme conditions: Pressure evolution of chemical bonding and structure in dense solids

Cite as: Matter Radiat. Extremes 5, 018202 (2020); doi: 10.1063/1.5127897
Submitted: 14 September 2019 • Accepted: 8 December 2019 •
Published Online: 16 January 2020

Choong-Shik Yoo[a)]

AFFILIATIONS

Department of Chemistry, Institute of Shock Physics, and Materials Science and Engineering, Washington State University, Pullman, Washington 99164, USA

[a)] csyoo@wsu.edu

ABSTRACT

Recent advances in high-pressure technologies and large-scale experimental and computational facilities have enabled scientists, at an unprecedented rate, to discover and predict novel states and materials under the extreme pressure-temperature conditions found in deep, giant-planet interiors. Based on a well-documented body of work in this field of high-pressure research, we elucidate the fundamental principles that govern the chemistry of dense solids under extreme conditions. These include: (i) the pressure-induced evolution of chemical bonding and structure of molecular solids to extended covalent solids, ionic solids and, ultimately, metallic solids, as pressure increases to the terapascal regime; (ii) novel properties and complex transition mechanisms, arising from the subtle balance between electron hybridization (bonding) and electrostatic interaction (packing) in densely packed solids; and (iii) new dense framework solids with high energy densities, and with tunable properties and stabilities under ambient conditions. Examples are taken primarily from low-Z molecular systems that have scientific implications for giant-planet models, condensed materials physics, and solid-state core-electron chemistry.

I. NOVEL STATES AND NEW MATERIALS UNDER EXTREME CONDITIONS

The materials that exist deep in planets and stars experience extremely high pressures (HPs) and temperatures (Fig. 1). The pressure spans tens of orders of magnitude, ranging from 0.1 to 1 GPa in icy comets to a few 100 GPa in earth-like rocky planets and 1–100 TPa in gas giants in solar and extra-solar systems.[1] The compression energy spans: (i) 1–10 meV for the dispersion and dipole energies, sufficient for the condensation of most, if not all, light gas molecules into liquids and solids; (ii) ~1 to 10 eV for the valence-electron energies, for chemical reactions to form extended polymers and metals; and (iii) a few 10–1000 eV, involving deep core electrons for new chemistry to occur.

Materials under extreme conditions undergo significant changes in their bonding, structures, and properties that have significant implications for the fundamental sciences, materials, and technologies. For example, the compression energy at the bottom of the ocean (~0.1 GPa) rivals the hydrogen bond energy that drives water to form clathrates with captured methane inside.[2] At 1–12 GPa, all light-gas molecules, such as H_2, He, N_2, O_2, H_2O, and CO_2 condense into highly compressible molecular solids. At 10–50 GPa, unsaturated chemical bonds become unstable compared with more saturated ones, converting *sp* hybridized C≡O, C≡N, and C≡C bonds to sp^2/sp^3 conjugated polymers[3–5] and sp^2 graphite to superhard sp^3 diamond.[6] At 50–100 GPa, the compression energy rivals or even exceeds the chemical-bond energies of C≡O and N≡N, two of the strongest chemical bonds in molecules. Under such conditions, all first- and second-row (or low-Z) elemental solids form dense covalent network structures, such as cubic gauche (*cg*)-N,[7–9] silica-like CO_2-V,[10–13] and symmetric ice-X.[14–16] At 200–500 GPa, many covalent solids become metallic, and even superconducting, as predicted and found in compressed H_2[17–19] and H_2S (attributed to H_3S).[20,21] Above 1 TPa, atoms are brought so close together that even the valence electrons of simple metals can assemble together as quasiparticles,[22–24] which fill the interstitial sites of core-electron nuclei and form the novel ionic states of electrides. Yet, at higher pressures of 10–100 TPa, the

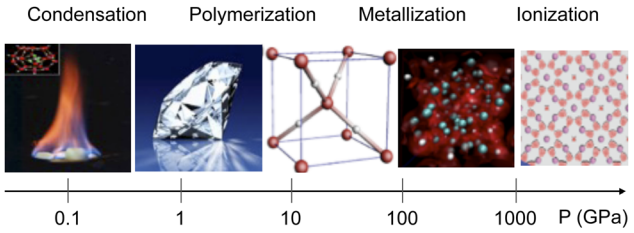

FIG. 1. Novel states of materials occur under a wide range of extreme pressures, which include methane hydrates at 0.1 GPa, diamond at 5 GPa, symmetric ice at 80 GPa, metallic hydrogen at 500 GPa, and Al electrides at 10 TPa. These pressures can be generated by modern high-pressure technologies in static and dynamic conditions (Fig. 2).

compression energy can reach that of the core-electron energy (1–10 keV), which may give rise to an entirely new chemistry.

High-pressure (HP) research examines the novel states, transformations, and properties of dense elemental solids that may constitute the interiors of giant planets and exoplanets. HP research provides fundamental materials data over a large range of pressure, temperature, and compression energy, which is critical to development and validation of new condensed matter theories and planetary models. HP research also provides fundamental insights into the stability-structure-property relationships of solids, which is critical to the development of new materials and structures that are stable at or near ambient conditions. In recent years, there has been an unprecedented number of discoveries of new materials and material structures, establishing pressure as a new dimension in materials research.[25–33]

In this paper, we present several fundamental concepts governing the chemistry of dense solids under extreme conditions, retrieved from the recent discoveries of new materials under extreme conditions. The focus will be on understanding the pressure-induced evolution of chemical bonding and structure in dense solids, from molecular to covalent, ionic and, ultimately, metallic solids under extreme conditions. We also focus on the novel properties and complex transition mechanisms arising from the subtle balance between electron hybridization (bonding) and electrostatic interaction (packing) in densely packed solids.

This paper is organized as follows: We first describe modern high-pressure experimental methods in Sec. II; then, we discuss the thermodynamic constraints on chemistry under extreme conditions, with reference to the pressure evolution of chemical bonding and structure in Secs. III–VII, and the kinetic constraints associated with the transformations in Sec. VIII. We also describe our recent efforts to develop new high energy density materials using dense, solid mixtures in Sec. IX. Finally, we offer some concluding remarks in Sec. X.

II. EXPERIMENTAL METHODS

Studies of highly compressible molecular solids under extreme conditions are very challenging for several reasons. These include: (i) the difficulties in achieving extremely high pressure-temperature (PT) conditions; (ii) the absence of an *in situ* structural probe in a small number of samples, inevitable at high static pressures; and (iii) the transient nature (sub-nanosecond) of the compressed states encountered at high dynamic pressures (Fig. 2). Nevertheless, with the recent developments in diamond anvil cells (DACs) coupled with micro-probing diagnostics at third-generation synchrotron x-ray sources and modern laser systems, these challenges are becoming less problematic. A DAC can routinely generate static pressures of 200–300 GPa, while DACs employing toroid diamond anvils[34,35] and double-stage diamond anvils[36] can reach 500–700 GPa—the realm of dynamic experiments using two-stage gas guns and high power lasers. Increasing effort has been made to use various large-volume presses for static HP materials research, employing WC anvils,[37] møssanite anvils,[38] sapphire anvils,[39] high-pressure sintered cBN anvils,[40] and polycrystalline diamond (PCD) anvils,[41] in combination with various hydraulic presses.

Dynamic-DAC[42–49] complements conventional DAC and shock wave experiments, capable of generating rapidly modulating pressures over a large range of pressure, strain and strain-compression rates. Furthermore, by applying a series of rapidly modulating

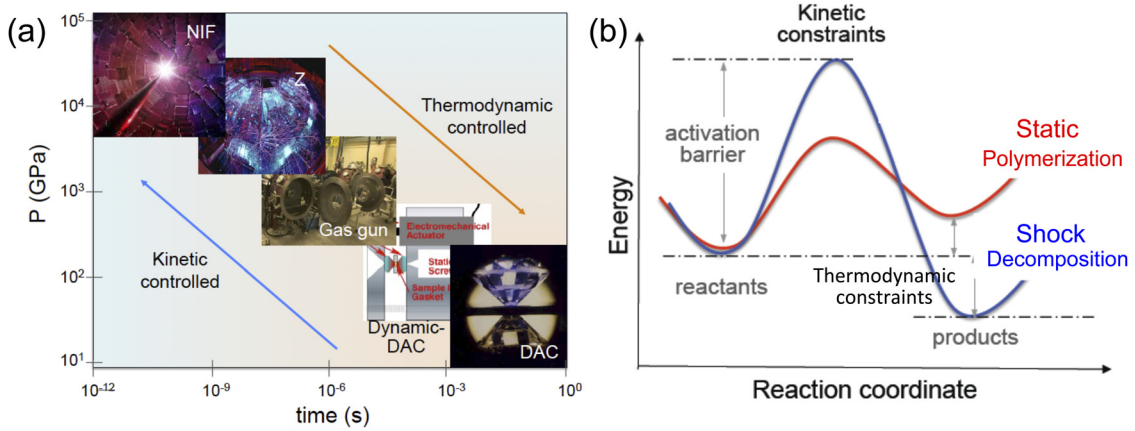

FIG. 2. (a) Modern high-pressure technologies, such as DAC, *dynamic*-DAC, gas guns, Z-machine, and NIF are capable of generating the extreme PT conditions in the deep interiors of the giant planets at different time scales. (b) Energy vs reaction coordination diagram, comparing kinetically constrained chemical processes between shock- and static-compressed materials, leading to decomposition and polymerization, respectively.

pressures in various functional forms, *dynamic*-DAC produces a controlled compressive shear at the interface, thereby enhancing chemical miscibility between the two dissimilar lattices of low-Z molecular solids. This method has been used in combination with time-resolved (TR) Raman spectroscopy,[45] TR x-ray diffraction,[46] high-speed optical microscopy,[47,48] and optical interferometry[49] to probe metastable structures, phase transitions, and chemical reactions, at tailored compression rates of up to 10^4 GPa/s.

Gas-guns, high-power lasers, and magnetic drivers are also used in HP research to investigate material behaviors under dynamic compressions. The Z-pulse power machine and high-power lasers, such as the Omega (Ω) and the National Ignition Facility (NIF), extend the limit of static pressures to dynamic pressures, well over 1 TPa.[50–52] The NIF, for example, is capable of attaining 1 PPa (10 Gbars) in low-Z materials in a convergent geometry,[53] where atoms in solids can be squeezed into the regime of the Bohr's radius. While dynamic experiments are typically performed to the Hugoniot state of a material,[54] they can be modified to provide an array of precisely controlled thermal loadings, ranging from double and multiple shocks to ramp-wave loadings and to quasi-isentropic states, thus enabling one to access a substantially wider range of phase space.[55,56] Furthermore, coupling with advanced light sources such as 3G synchrotron x-rays[57,58] and 4G x-ray free electron laser (XFEL),[59,60] it is now possible to investigate the fast transformations and transient species of shocked materials in time scales of nanosecond to femtosecond.

Shock and static high pressures are complimentary in many aspects, including in thermal conditions, kinetics, states of stress, and rates of loading; all of these can affect material transformations (Fig. 2). Because of these differences, materials behave quite differently under shock and static conditions. For example, shocked materials undergo shear driven martensitic transformations[61] than thermodynamically bound reconstructive ones. Shock-compressed liquid is often found well above its melt curve,[62] typically crystallizing into nanocrystals or amorphous materials.[63] Shock-induced reactions are often dissociative, leading to decomposition products,[64] whereas static reactions are typically associative, leading to polymeric products[65,66] [Fig. 2(b)]. Shock compression occurs along uniaxial strain, enhancing shear-band interaction in a solid,[67] which is absent in static conditions.

The complementary information from shock- and static-high-pressure experiments is critical to gain insight into material transformations at high PT conditions. Furthermore, combining these static and dynamic HP methods with advanced light sources, such as third-generation (3G) synchrotron x-rays, 4G x-ray free electron lasers (XFELs), and spallation neutron sources (SNS), provides opportunities to discover new materials and exploit new chemistry under extreme PT conditions.

III. STRUCTURE AND CHEMICAL BONDING

The nature of chemical bonding in a dense solid under extreme conditions can be quite different from that under ambient conditions, a nature manifested in the solid's crystal structure. An excellent example of this is the nearly identical density between noble gas solid Xe and ionic solid CsI above ~80 GPa–300 GPa,[68,69] while displaying completely different densities and chemical bonding at ambient and low pressures. It underscores the chemistry occurring in these very different solids and leads to very similar if not identical chemical bonding. It is important to note that both Xe[70,71] and CsI[72–74] become metallic at around 110–130 GPa, and questions are emerging regarding the exact nature of the related chemistry, the answers to which could apply to other materials under similar conditions: how do different chemical bonds in solids [including van der Waals (vdW), covalent, and ionic bonds] evolve into metallic states; where do they occur; and what drives such changes?

To illustrate the pressure-induced evolution of structure and chemical bonding under extreme pressures, we consider a hypothetical 2D molecular lattice in Fig. 3.[28] Molecular solids are highly compressible, bound by weak van der Waals interactions. Upon compression the vdW space is rapidly collapsed, and the nature of intermolecular interaction becomes highly repulsive. As a result, the electrons localized within intramolecular bonds become unstable, inducing pressure-induced electron delocalization among adjacent molecules. This results in the transformation of molecular solids to nonmolecular extended solids in the three-dimensional (3D) networks of corner (or edge)-sharing polyhedra. Examples are numerous, including single bonded "polymeric" *cg*-N[7–9] and silica-like CO_2-V.[10–13]

Extended solids initially possess high-symmetry open structures, with highly degenerated atomic configurations, as found in diamond and symmetric ice X. With increasing compression, these open network structures are subjected to subtle structural symmetry-breaking distortions, which are electronic in origin. The driving force for symmetry lowering transitions is densification achieved by polarizing the chemical bonds. The consequence of structural distortion is, however, many near-ground states, providing pathways to local energy minima, path-dependent transitions, and phase metastability, as observed in layered polymeric nitrogen (LP-N)[75,76] and layered carbonate (i-CO_2)[77] structures.

Upon further compression, to well above 100 GPa, the valence electrons of low-Z extended solids may ionize to form an ionic solid or a mixture of substituent elemental solids. Pressure-induced ionization occurs as electrostatic forces begin to dominate at extreme conditions.

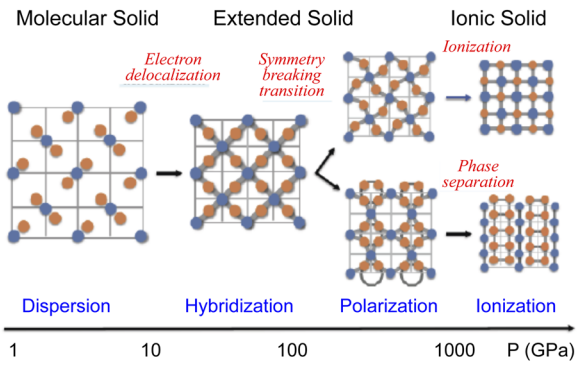

FIG. 3. A concept of pressure-induced chemistry in a 2D lattice, illustrating the evolution of chemical bonding and structure with increasing pressure, from weakly bound molecular solids to covalently bonded extended solids and ionic solids. These transformations are primarily driven by pressure-induced densification, promoting the delocalization and even ionization (or localization) of electrons from both valence and core states [Reproduced with permission from C.-S. Yoo, MRS Bull. **42**, 724 (2017). Copyright 2017 Cambridge University Press].

At a given density, a delicate balance between electron delocalization (governing bonding) and ionization (governing packing) can give rise to novel structures and phenomena. Important properties resulting from this balance between bonding and packing include kinetic-controlled transformations, novel interfacial structures, and large bandgap ionic solids.

The HP chemistry described above occurs at large compression energies,[26,27] exceeding the energies of defects and grain boundaries that make the solid-state reaction nonpredictive and uncontrollable under ambient conditions. In this regard, the structure of dense solids is predictive, primarily based on thermodynamic constraints. This makes possible the development of new materials from the stages of computational design to experimental discovery, and vice versa.[28–31]

IV. PRESSURE-INDUCED ELECTRON DELOCALIZATION TO EXTENDED COVALENT SOLIDS

Pressure-induced transformations from dense molecular solids to nonmolecular extended solids with strong covalent-bond frameworks reveal a fundamental principle of high-pressure chemistry; that is, pressure-induced electron delocalization, which occurs because electron kinetic energy has a higher density dependence ($\rho^{2/3}$) than does electrostatic potential energy ($\rho^{1/3}$). As a result, electrons localized within intramolecular bonds become increasingly less stable as density (or pressure) increases, and the intermolecular potential becomes highly repulsive. At high enough pressures, this leads to more electron-delocalized states, such as polymeric or metallic solid states. This is the reason that many unsaturated molecular bonds become unstable at pressures of 10–20 GPa,[78–80] and fully saturated single-bonded 3D network structures are ubiquitous at high pressures.[81]

The pressure-induced electron delocalization in dense molecular solids can be understood in terms of storing large compression energies into chemical energies in dense framework structures. The resulting materials typically have high densities (3–4 g/cm^3) and high energy densities (1–10 eV/nm), constituting a high-energy-density solid (HEDS). Because a HEDS is made of strong covalent bonds, there can be a large kinetic barrier to depolymerization, providing opportunities to recover them at ambient conditions. This is illustrated in Fig. 4. Observing the transition at the onset of transition threshold pressure typically requires the substantial heating of materials, despite their expected stability at lower temperatures. For example, the graphite-to-diamond transition occurs above 1500 °C at 5 GPa,[82] yet is absent, or occurs at substantially higher pressures,[75,83,84] at ambient temperatures. Instead, compressing graphite at ambient temperature leads to highly disordered solids above 20–40 GPa.[76,85]

Nitrogen was the first element predicted to form singly bonded *cg*-N,[7] later confirmed by laser-heated DAC experiments.[8,9] This polymerization is accompanied by a huge volume collapse ~25%, even at 110 GPa,[86] which is remarkable in comparison with the graphite-to-diamond transition, ~27% at 5 GPa.[87] The calculation predicts that *cg*-N is a HEDS with an energy content of 33 kJ/cm^3, as well as its being recoverable under ambient conditions. The depolymerization activation barrier is estimated to be 1.2 eV/atom. However, *cg*-N reverts to molecular N_2 below 60 GPa.[8,9,88] This apparent discrepancy is likely due to the catalytic effect of surface atoms, unzipping (or depolymerizing) the network structure, as found in CO_2-V.[89]

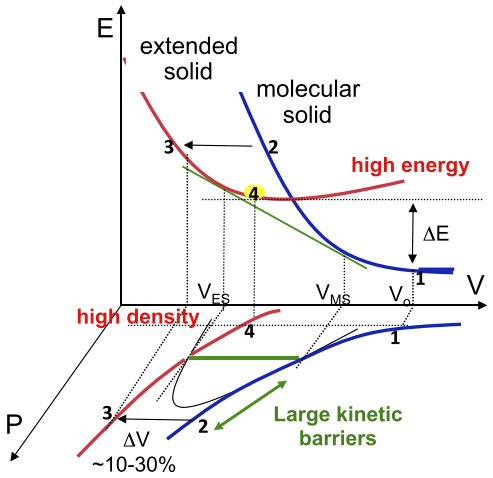

FIG. 4. A thermodynamic representation of pressure-induced electron delocalization to high density, high energy extended solids. V_o signifies the specific volume of molecular solid under ambient conditions, whereas V_{ES} and V_{MS} represent the molecular solid and extended solid at the transition pressure. The pressure (or energy) offset of the transition (2 → 3) from the equilibrium value (the green line) signifies the presence of a large activation barrier. A similar kinetic barrier in the backward transition (3 → 4), on the other hand, makes it possible to recover the high-energy, high-density product under ambient conditions.

Low-Z extended solids exhibit many interesting mechanical, optical, and electronic properties, in addition to high energy density, and constitute a class of novel materials. Some examples are shown in Fig. 5; note the substantial level of second harmonic generation by silica-like CO_2-V,[90] the high critical temperature (Tc) superconductor of dense CS_2,[91,92] the high energy density of CO,[93] and the colossal Raman cross section of LP-N.[75] These properties of extended solids arise from the combination of their being low-Z and comprising dense 3D network structures. The large cohesive energy, E, and small interatomic distance, d, for example, make low-Z extended solids extremely incompressible, as evidenced by their large bulk moduli, B, where it can be approximated as ~E/d.[94,95] Furthermore, at high pressures π– or nonbonding electrons in unsaturated low-Z molecules are more accessible than σ-electrons, resulting in all singly bonded network structures possessing large bandgap energies, as does diamond and *cg*-N. The high phonon frequencies of low-Z lattices can more efficiently couple with electrons, resulting in high Tc superconductivity,[96] while the high thermal diffusivity of low-Z lattices renders extended solids more resistant to extreme heat and photon flux. The collective behavior of electrons, phonons, and ions, in such continuous low-Z 3D network structures, results in new functionalities, such as piezoelectricity, ferromagnetism, superconductivity, superionicity, and nonlinear optical behavior, underscoring the considerable potential of low-Z extended solids.

V. PRESSURE-INDUCED ELECTRON LOCALIZATION TO LOW SYMMETRY IONIC SOLIDS

The formation of nonmolecular extended solids produces relatively highly symmetric local structures of corner-shared polyhedra. With regard to density, these are relatively open structures that are

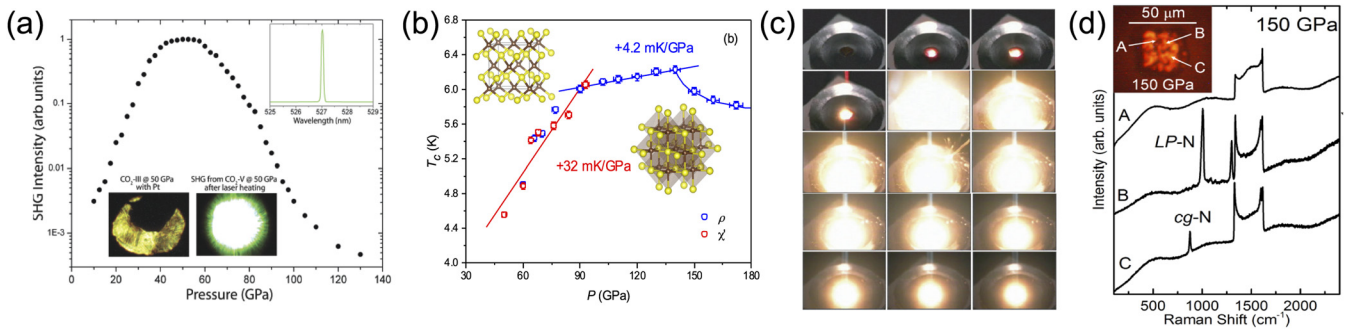

FIG. 5. Novel properties observed in low-Z extended solids: (a) Second harmonic generation of silica-like CO_2-V. (b) Superconductivity of dense CS_2. (c) High energy density of polymeric CO. (d) Colossal Raman scattering of layered polymeric nitrogen (LP-N) [Reproduced with permission from C.-S. Yoo, MRS Bull. **42**, 724 (2017). Copyright 2017 Materials Research Society].

eventually subjected to lattice distortions in tighter spaces or under further compression, to pressures well above 100 GPa. Driven by densification, the valence electrons of extended solids may become highly polarized and even ionized to form ionic solids, as the columbic attraction supersedes the stabilization of electron delocalization (bonding) at small interatomic distances. As a result, the high-symmetry extended solids in the 3D covalent networks transform into ionic solids with highly distorted, low-symmetry and low-dimension structures, as predicted and observed in H_2O, N_2, CO, and CO_2 at high pressure.

Evidence for pressure-induced ionization can be found in the layered structures of dense solids at extreme pressures (Fig. 6). Nitrogen, for example, is a prototypical diatomic molecule, exhibiting a fascinating polymorphism with four solid molecular phases (α, β, γ, δ) below 10 GPa and 300 K.[88,97,98] Upon compression, δ-N_2 undergoes a series of structural transitions to ε-, ζ-, and amorphous black η-N_2 at ambient temperature, and to ε-, θ-, and amorphous "*red*"-N at high temperatures.[9,99–101] These phases in the intermediate pressure range exhibit strong kinetic dependence, such as path-dependent stability, metastability, large lattice distortions, and irreversible transformation.[102] At 120–180 GPa, nitrogen becomes fully saturated (or extended), first forming singly bonded *cg*-N ($I2_13$) at 110 GPa,[8,9] and then, 2D layered polymeric LP-N (*Pba*2) at 120–180 GPa.[103] Interestingly, the LP-N structure is made from two different nitrogen atoms; one in a nearly ideal (<NNN = 120°, sp^2-hybridized) three-fold coordination, and the other in a buckled (<NNN = 100°, sp^3-hybridized) three-fold coordination, analogous to that in *cg*-N.[104,105] This structure clearly indicates the polarization of nitrogen, resulting in the distorted, layered structure at high density (~4.85 g/cm^3 at 120 GPa). In comparison, the density of *cg*-N is 4.50 g/cm^3 at the same pressure. The layered structure gives rise to two distinctive nitrogen vibrational modes from the sp^2 N-N at 1300 cm^{-1} and the sp^3 NN at 1000 cm^{-1} at 150 GPa. The latter mode is analogous to that of cg-N at ~900 cm^{-1} at the same pressure, considering a ~7.8% density difference between *cg*-N and LP-N. The formation of singly bonded layered nitrogen has recently been confirmed even at the higher pressures of 180–250 GPa, noted as HLP-N.[106] Thus, the symmetry lowering transition from 3D *cg*-N to 2D LP/HLP-N clearly underscores the pressure-induced ionization, which is driven by densification. In fact, the theoretical calculation[104,107] even predicts that 2D LP-N transforms to 0D N_{10} clusters with substantially enhanced ionic characters, evident from the greater diversity in the hybridization of nitrogen atoms, including the bonded sp^2 and sp^3 orbitals, as well as the lone pair, sp^3 and p_Z.

The formation of similar, layered structures has also been observed in dense CO, but at substantially lower pressures of 50–100 GPa.[108–112] Molecular CO (δ-phase) undergoes a series of chemical transformations: initially to a highly colored, low-density (~1.8 g/cm^3) polymeric phase I at 6 GPa,[91] then to a higher density (~2.4 to 3.4 g/cm^3) translucent 3D network, phase II, and finally, to a transparent, layered phase III, above 50–70 GPa.[113] The properties of polymeric CO phases are consistent with those of the theoretically predicted structures of dense CO phases:[113–115] 1D $P2_1/m$ for phase I, 3D $P2_12_12_1$ for phase II, and 2D *Cmcm* for phase III. Thus, these transitions in dense CO signify a stepwise polymerization of C≡O in the molecular phase to highly conjugated, unsaturated C=O in the 1D polymer in phase I, saturated C–O in the 3D network in phase II, and a 2D layered structure in phase III. The layered structure is evident from the characteristic nm-lamellar structure of recovered phase III.[108]

The evidence of pressure-induced ionization is found not only in molecular solids, CO and N_2, with unsaturated bonds, but also in singly bonded H_2O [Fig. 6(c)][116–118] and ionic solids, like NaCl [Fig. 6(d)].[119,120] At ambient temperature, water crystallizes into a hydrogen-bonded network structure of ice VI ($P4_2/mnc$) at ~0.9 GPa, ice VII ($Pn3m$) at 2.1 GPa, and then, symmetric ice X (Pn-3m) at 40–80 GPa. The crystal structure of ice X is a 3D network made of highly symmetric corner-sharing OH_4 tetrahedra, where H atoms are at the center positions of two adjacent O atoms with <OHO = 180°. This is an open structure, which can be distorted upon further compression for the sake of achieving higher density. Molecular Dynamics (MD) simulations[118] have, in fact, predicted that the high symmetry proton-ordered ice X becomes unstable and transforms into a fast-ion proton conducting ice XI (*Pbcm*) at 300–400 GPa. Recent density functional theory (DFT) calculations[116,117] have predicted several additional phases in distorted layer structures: a $Pmc2_1$ phase at 930 GPa and a layered $P2_1$ crystal structure at 1.3 TPa [Fig. 6(c)]. These phases are wide-bandgap insulators over a large pressure range, up to 4.8 GPa, where it transforms to a metallic $C2/m$ phase.[116]

The low-pressure B1 ($Fm3m$ or cF8) phase of NaCl transforms into a *CsCl*-like B2 ($Pm3m$ or cP2) phase at ~30 GPa,[119] which is stable, at least to 304 GPa.[120] These phases are relatively high-symmetry structures, of which the band structures clearly indicate insulators with valence electrons localized on Cl^- anions. At higher pressures, the DFT

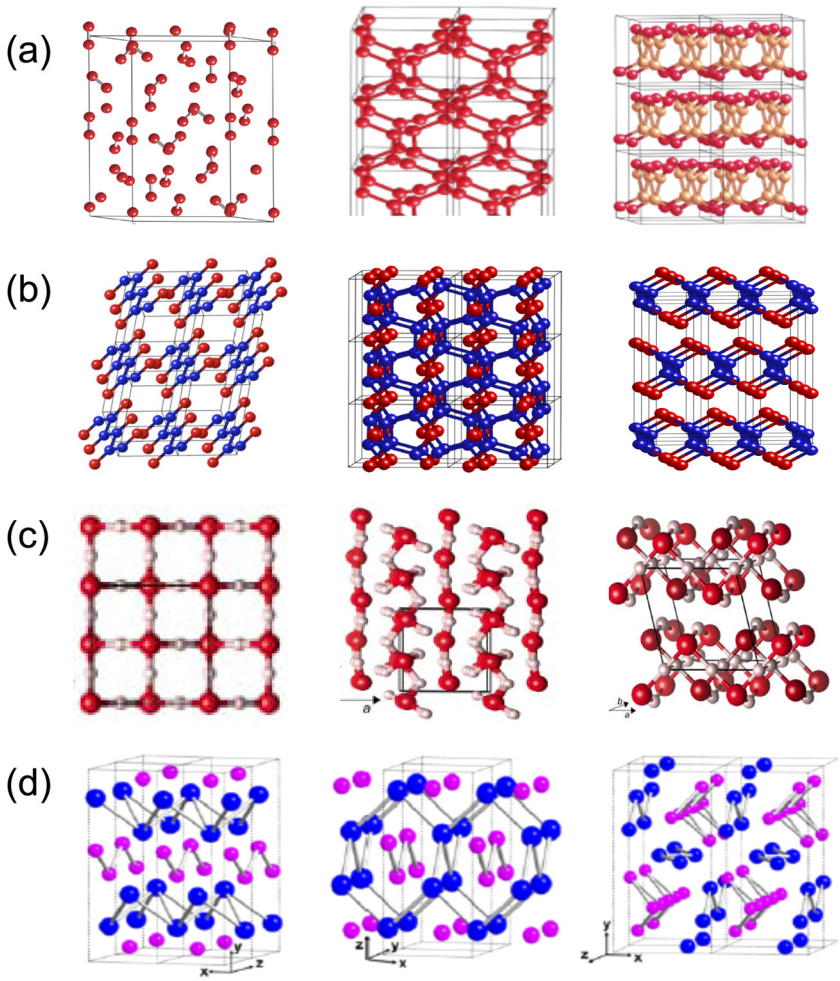

FIG. 6. Crystal structures of dense low-Z solids under extreme conditions, showing the pressure-induced ionization of 3D covalent bonds to 2D ionic solids in: (a) N_2 from the molecular ε(*r*-3*m*) phase to the singly bonded phase, 3D *cg*-N ($I2_13$) at 110 GPa, and 2D layered polymeric LP-N (*Pba*2) at 150 GPa. (b) CO from 1D linear chain phase I ($P2_1/m$) to 3D ladder phase II ($P2_12_12_1$) and 2D layered phase III (*Cmcm*). (c) H_2O from 3D symmetric ice X (*Pn*-3*m*) at 80 GPa to distorted $P2_1$ phase at 1 TPa and 2D layered *C*2/*m* at 2 TPa. (d) NaCl from an *oC*8 phase at 320 GPa to *oI*8 at 650 GPa and oP14 above 700 GPa.

calculations have predicted the stability of three new orthorhombic phases:[121] oC8 at 320 GPa, oI8 at 680 GPa, and oP16 at 700 GPa [see Fig. 6(d)]. It is important to note that these structures are distorted layer structures of Na^+ and Cl^- sublattices, which attain the required higher density compared with the low pressure phases, while maintaining their ionic characters up to around 1 TPa.

Clearly, there is abundant evidence for pressure-induced ionization to form low-symmetry, yet high-density, layered structures in dense solids, regardless of the nature of the chemical bonding that includes those existing as molecular solids, ionic solids, and even noble-gas solids at low pressures. Therefore, it is conceivable that the symmetry lowering transition from a 3D framework structure to a 2D layered structure occurs more often, in general, following the formation of extended covalent network solids. It arises from a substantially enhanced electrostatic (i.e., coulombic) interaction in densely packed solids at extreme pressures, well above 100–300 GPa. In fact, the formation of simple metal electrides[22–24] can be considered in a similar way: valence electrons by themselves form anions, filling in the interstices of the protonic sublattice in low-symmetry structures.

VI. METALLIZATION OF IONIC SOLIDS

One important question is whether an ionic state, such as pressure-induced ionization, could ever be metallized? If so, when (pressure), how (mechanism), and where (states) would it transform? This is a crucial but unresolved question in relation to most materials because of experimental limitations in achieving those extreme conditions that are only within the realm of theory. Nevertheless, the metallization of ionic solid CsI in comparison with the van der Waals noble-gas solid Xe may offer some insights into the chemical mechanism of metallization in dense ionic solids. For example, the B2 (*Pm*3*m*) phase of CsI transforms into an orthorhombic (*Pnma*) phase at 42 GPa, with a hexagonal, closed packed (*hcp*) stacking,[72] resembling *hcp* Xe. Furthermore, CsI becomes

metallic above 115 GPa, and even superconducting above 180 GPa, at a critical temperature of ~2 K.[73] Interestingly, theory[74] explains that the superconductivity originates from an electron transfer from I^- to Cs^+, resulting in the same closed electronic-shell configuration of Xe. In fact, Xe becomes metallic at 132 GPa, although no superconducting transition has been found in pure Xe.

It is important to note that, despite the closed-shell structure, valence electrons in Xe are highly polarizable, which can give rise to a wide range of chemical compounds.[122–124] Thus, a plausible, alternative mechanism that explains the similar metallic bonding in CsI and Xe above 110–130 GPa[70–74] is a charge transfer mechanism between Xe atoms, forming an ionic solid, consisting of partially charged Xe^+ and Xe^- layers, analogous to the pressure-induced ionization in CO, N_2, and H_2O [see Fig. (6)], as well as the structure of the layered *hcp*-like structure of CsI. Metallization can then occur by closing the bandgap of the anionic Xe sublattice. This mechanism of metallization is then analogous to what has been predicted to occur in NaCl above ~700 GPa [Fig. 6(d)].[121]

In NaCl [Fig. 6(d)], theory predicts that the oC8 structure is metallized via pressure-induced bandgap closure above ~650 GPa, while both oI8 and oP16 are metallic in their stable pressure ranges above ~700 GPa. Interestingly, the calculated band structures indicate that all predicted metallic phases retain predominantly ionic characters up to 900 GPa, whereas the metallic properties are primarily due to the band overlap of hybridized Cl 3*p*-3*d* states. Calculations show that the DOS of Na near the Fermi level is very low in these phases, highlighting the charge transfer from Na to Cl and the ionic character in these phases. Therefore, the metallic behavior of these ionic phases can be attributed to the crystal structures of the extended anionic sublattices. The ionic attraction between layered sublattices certainly favors electron conductivity.

Novel metallic states are also expected to form from dense ionic phases of N_2 and H_2O ($P4_1$), but at even higher pressures. The metallic state of solid N_2 has not yet been predicted, although increasing optical reflectivity has recently been reported in fluids above 2500 K and 125 GPa[125,126] in the pressure regime of *cg*-N and LP-N. The distortion of dense symmetric H_2O induces polarization in O–H–O bonds, breaking up the typical tetrahedron bonds and forming a partially ionized phase ($P2_1$) consisting of coupled charge transferred layers of $(OH)^-$ and $(H_3O)^+$ lattices [Fig. 6(c)]. This ionic phase is predicted to transform into a metallic $C2/m$ phase at 4.8 TPa,[116] resulting from a pressure-induced band overlap of the O^{2-} sublattice. This mechanism of metallization—by closing the bandgap of the anion sublattice—is, again, analogous to that of NaCl and Xe conjectured above, and thus provides a general picture of the chemistry in dense solids. The same theory predicts that at 4.8 GPa the zero-point energy of hydrogen is substantially greater than the binding energy of the lattice, causing the melting of the H-sublattice or even the entire solid. Such a remelting in dense H_2O is similar to that observed in H_2 and alkali metals, such as Li[127,128] and Na,[129] as well as in the dissociation of hot dense H_2O and NH_3 reported in MD simulations[130] and recent experiments.[131] These mechanisms, however, can compete with the metallization of ionic phases of H_2O, depending on a subtle balance between the collapsing of the electron bandgap of the oxygen sublattice and kinetically controlled proton diffusivity.

VII. TEMPERATURE-INDUCED IONIZATION

Increasing temperature expands the bond distance in more open structures like bcc because of a large increase in entropy[132] and ultimately induces the formation of ionic species,[133,134] as illustrated in Fig. 7. Such a temperature-induced ionization would eventually produce a conducting state of matter if the pressure was sufficiently high.[56,135] This means that the molecular-to-nonmolecular and insulator-to-metallic transitions would form a closed loop in the pressure-temperature phase diagram. These close loops of melting and molecular-to-nonmolecular phase lines should intersect at a triple point of intermediate high pressure and temperature.[136,137] Therefore, the combined effects of high pressure and high temperature provide a way of probing the delicate balance between mechanical (PΔV) and thermal (TΔS) energies, or between pressure-induced electron delocalization and temperature-induced electron ionization, reflected by the stabilities of phases and phase boundaries. These pressure-temperature induced changes are unique, establishing an entirely different set of periodic behaviors in crystal structure and electronic and magnetic properties not found in the conventional periodic table.

At high temperatures, materials can increase their fluidity (or diffusivity) by a substantial degree, especially if they are light elements, such as H and He, and form novel superionic states of dense solid H_2O and NH_3, where hydrogen atoms can move freely, while oxygen atoms are fixed in their anionic sublattice. Recently, it has been predicted that He and H_2O can also form stable compounds, such as $He(H_2O)_x$ where x = 1, 2, 3,. . . over a large pressure range—even close to ambient pressure.[138,139] Interestingly, *ab initio* MD simulations indicate that $He(H_2O)_x$ transforms to novel superionic phases at

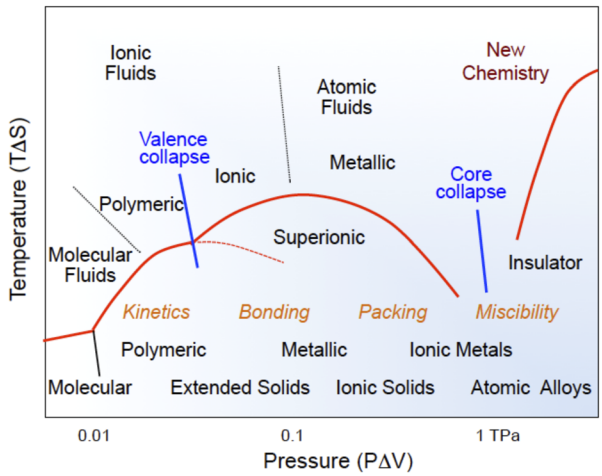

FIG. 7. A conceptual phase/chemical transformation diagram of molecular solids, signifying the pressure and temperature induced ionization leading to nonmolecular polymeric, metallic, and ionic solids. A delicate balance between the compression energy (PΔV) and the entropic energy (TΔS) under extreme pressure-temperature conditions gives rise to novel states and transitions of materials in both solids and liquids, which are strongly controlled by chemical kinetics. The compression energy at 100 GPa (~10 eV) can strongly modify the valence electron configuration or chemical bonds of molecular solids; at 1 TPa (~100 eV) it can even alter the core electron configuration and induce a new type of chemistry never experienced in the past.

elevated temperatures, initially He-disordered then H-disordered at the interstices of the ordered oxygen lattice, before the melting or disordering of the lattice[138] The formation of superionic phases of light elemental solids is important, as they form under the PT conditions of the ice layer in giant planets. Furthermore, the predicted demixing of H_2 and He[140] can give rise to He precipitates in H_2O in the ice layer and thereby alter the structure, composition, and dynamo of planets.

VIII. KINETIC-CONTROLLED TRANSFORMATIONS

Kinetically controlled processes provide opportunities to observe metastable phases and develop new materials, both crystalline and amorphous solids, under rapid compression using *dynamic*-DAC and rapid quenching using laser-heated DAC, as well as by shock compression using gas guns and high-power lasers. This approach stems from the fact that the dynamic shear strains generated by rapid yet precisely controlled pressure (or temperature) modulations can enhance interfacial mixing and thereby the chemistry between the dislike lattices of C, B, N_2, H_2, and O_2. Furthermore, by precisely controlling pressure, large crystals can be grown along the melt boundary into different crystal morphologies, including single crystals, fractals, and dendrites, by varying the characteristics of pressure modulation, and the shape, frequency, amplitude, and compression rate. This is observed during the solidification of water, as shown in Fig. 8.[42,43,47] Image A shows a single crystal and B dendrites, although both are made of ice VI.[42,43] Liquids can be rapidly compressed to super-compressed states to produce metastable structures that may resemble the structure of dense liquids, e.g., metastable ice VII is produced in the stability field of ice VI, shown in image C. Various forms of disordered solids can also be formed, such as the high-density amorphous ice produced in no man's land in image D.[47] While crystal growth mechanisms are important in understanding the *macroscopic* complexities of crystal morphologies and microstructures, they are also important in understanding the *microscopic* behaviors of atoms and molecules at solid-liquid interfaces.

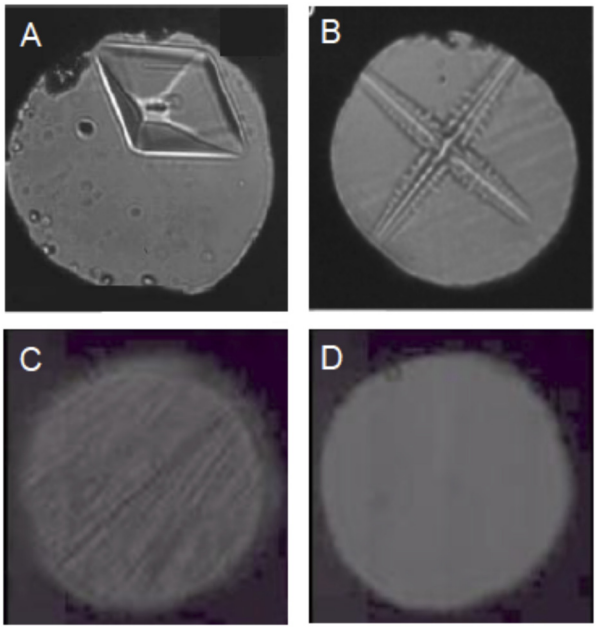

FIG. 8. Various ice crystals, stable and metastable, formed along different thermal and kinetic path under rapidly modulating pressures using *dynamic*-DAC, including (a) single crystal ice VI (b) dendritic ice VI (c) metastable ice VII produced in the stability field of ice VI, and (d) high density amorphous (HDA) ice produced in no man's land.

The transition mechanisms of dense solids are generally complex and often controlled by strong kinetics, especially in the transition regions of: (i) Structural miscibility at relatively low pressures,[141–144] where atomic and molecular diffusion are very much limited, and the chemistry is controlled by structural miscibility and lattice strain at the interfaces. This is important in understanding the chemistry at the interfaces of heterogeneous mixtures that leads to low-dimensional modulated structures, such as solid H_2 intercalated graphite.[145] (ii) Chemical bonding in an intermediate pressure region, where molecular solids develop substantial intermolecular interaction, greater than that between hydrogen bonds but less than that between covalent bonds. The transformations are controlled by kinetics, thermal paths, and lattice distortions, well beyond thermodynamic constraints. Examples include the path dependent phase boundaries between CO_2-II and CO_2-IV,[146] as well as the path-dependent phases of CO_2-VI[147] and coesite-like CO_2.[148] (iii) Electrostatic packing in a high-pressure region, where electron hybridization (bonding) energy competes with electrostatic stabilization (packing) energy, and high-symmetry 3D network structures transform into low-symmetry distorted structures, eventually leading to ionization, decomposition, or phase separation. This packing effect is important in understanding the chemistry in immiscible mixtures that results in nonstoichiometric interstitial-filled compounds. These are the regions where a profound knowledge gap exists in both theory and experiment under extreme conditions. Thus, future high-pressure studies should examine the behavior of materials in these transition areas in both the unary and binary systems of low-Z molecular solids.

IX. DENSE FRAMEWORK SOLIDS WITH HIGH CHEMICAL ENERGIES

Discoveries of novel low-Z extended solids at high pressures have opened up new avenues of research inquiry. While these covalently bonded extended framework solids exhibit unusual properties, such as high energy density, extreme hardness, second harmonic generation, a colossal Raman cross section, and a record high T_c superconductivity (Fig. 5), these materials revert to their molecular states upon the release of pressure, thus losing their novel properties. As a result, only a few systems have been recovered to date, limiting the materials within a realm of fundamental scientific discoveries. Therefore, an exciting new research area has emerged regarding understanding and, ultimately, controlling the stability, bonding, structure, and properties of low-Z extended solids in various novel framework structures.

The development of low-Z extended solids amenable to ambient stabilization poses great scientific and technological challenges. Those challenges primarily stem from the formidable transition pressures and high-energy states, which make them metastable at low pressures. A logical way to overcome these challenges is to use low-Z solid

mixtures, where the internal chemical pressure can lower the transition pressure, and strong hetero-nuclear chemical bonding replaces dangling bonds, enhancing the stability of extended network structures under ambient conditions. Furthermore, a greater number of new materials can potentially be developed via solid-state combinatory reactions of mixtures. Importantly, the use of mixtures permits the control of the transition pathway and pressure, and of the stability, structure, and properties of products.

The novel properties of extended solids (Fig. 5) are, to a first approximation, controlled by interatomic distance and topological arrangement (or framework structure), both of which can be tuned precisely and significantly by pressure and composition. Consequently, the properties of extended solids made of binary and ternary mixtures can be as novel as those of single-component low-Z extended solids, yet can be tuned chemically using various elemental solids or specific extended structures. Examples include an array of polymeric products formed from dense CO mixtures with H_2, N_2, and Fe, as described below.

CO:[108] Carbon monoxide was one of the first molecular systems found to transform into a highly disordered and colored (brown-dark red) nonmolecular "polymeric" solid above 5.5 GPa that can be recovered at ambient pressure.[109–112] Recently, it was found that this dark-brown polymeric CO solid (pCO-I or phase I) undergoes further chemical transformations, initially to translucent pCO-II at 11 GPa, and then transparent pCO-III above 50 GPa, which is stable over a wide range of pressures, at least to 160 GPa.[108] These high-pressure transformations in CO clearly highlight an interesting structure-bonding relationship of C≡O in the molecular phase to C=O in the 1D chain of pCO-I, and C–O in the 3D network of pCO-II and the 2D layer of pCO-III, as suggested in theoretical studies.[113] However, all recovered phases are deeply colored brown to dark red [see Figs. 9(a)–9(c)] and unstable at ambient conditions. The phases are hygroscopic and photoreactive, and they decompose to CO_2 and C. The density was measured ~1.8 g/c^3, suggesting that the recovered products are mostly pCO-I, although the distinctive changes in texture and color with changing synthesis pressure indicate the presence of pCO-II.

CO+H_2:[149] Doping carbon monoxide with hydrogen can greatly lower the polymerization pressure and enhance the stability of recovered polymeric products. For example, the deeply colored polymer (pCO-I) is formed at ~4 (5.5) GPa, which transforms to translucent pCO-II at 7–8 (10–12) GPa and then transparent pCO-III at 20–30 (50–70) GPa. The transition pressures in pure CO are noted in parentheses. All polymeric phases are recoverable at ambient conditions, exhibiting an array of phase stabilities and novel properties. For example, the products recovered from 5 to 6 GPa (mostly pCO-I) are highly unstable and rapidly sublime or decompose, leaving a small residue of yellow products. On the other hand, the products recovered from 7 to 11 GPa are substantially more stable with respect to pCO-I. The density of recovered products ranges from ~2.7 g/cm^3 to 3.2 g/cm^3 depending on the pressure recovered, indicating that they are mostly pCO-II. In fact, the recovered products show strong luminescence [Figs. 9(d) and 9(e)], which is characteristic of pCO-II. They are still highly disordered and slowly decompose into crystalline solids of anhydrous polymeric oxalic acid, while exhibiting interesting crystal morphologies, such as nm-cobs, nm-lamellar layers, and μm-bales.[149]

CO+N_2:[150] The synthesis of novel extended forms of nitrogen and nitrogen-rich materials has been a topic of interest in the development of high energy density materials.[151–154] Yet, the formidable transition condition of this type of synthesis (above 110 GPa and 2000 K) makes it impractical, if not impossible. Recent theory, however, has shown that in CO–N_2 mixtures, CO catalyzes the dissociation of N_2, which leads to 1D copolymers below 18 GPa and 3D networks at 52 GPa.

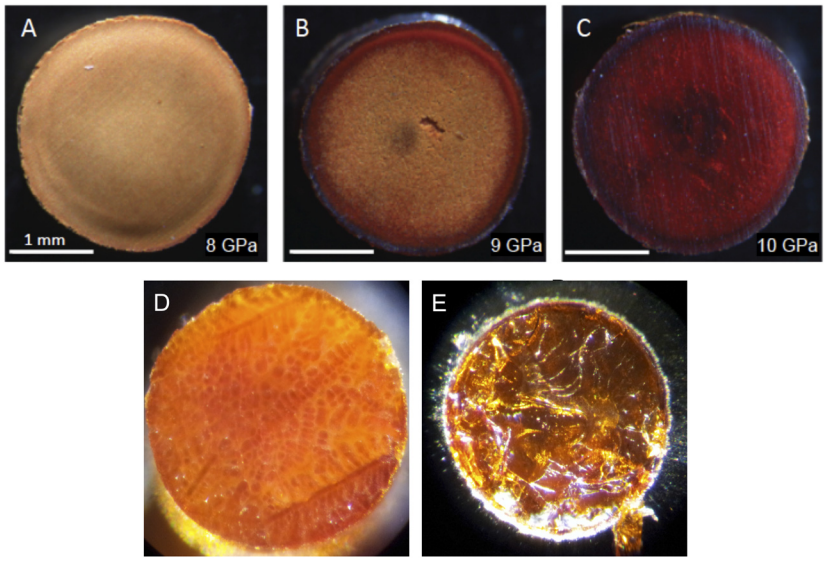

FIG. 9. Photographic images of polymeric carbon monoxide (pCO) products under ambient conditions, recovered after synthesis at high pressures: (a)–(c) pure pCO synthesized at 8, 9, and 10 GPa. The images show the presence of two polymeric products (I and II) (d) and (e) 10% H_2 doped pCO synthesized at 6 and 7 GPa, showing lower synthetic pressures than pure CO and strong luminescence [Reprinted with permission from Y. J. Ryu *et al.*, J. Phys. Chem. C **121**, 10078 (2017). Copyright (2017) American Chemical Society].

In fact, subsequent DAC laser-heating experiments have shown the formation of high-density (3.983 g/cm^3) copolymer CON_2, formed in crystalline form by laser heating of CO–N_2 mixtures above 1700 K and 45 GPa (Fig. 10)—a substantially lower pressure-temperature condition than is required for converting pure nitrogen. In fact, a disordered product can be made even at lower pressures ~20 GPa at ambient temperature. According to the refined structure shown in the inset of Fig. 10, the crystalline polymer is made of hybridized nitrogen, eight membered rings of singly bonded CON_2 in a three-dimensional framework structure in the space group of $P4_3$, one of the previously predicted structures.[155–158] However, unlike the predicted structures, the present $P4_3$ solid reverts to ε-N_2-like and δ-N_2-like molecular phases as pressure decreases to 20 and 10 GPa, respectively.

The formation of CON_2 copolymer strongly suggests that a concerted reaction mechanism is in play [Fig. 8(b)], which should involve a lower kinetic energy barrier than a reconstructive energy barrier, to form nonstoichiometric cross products of stacked *Fdd*2 and framework *Pbam*. The presence of organized dipoles and active reaction sites in solid CO can minimize the specific volume of the transition states toward copolymerization with nitrogen and, thereby, lower the reaction barrier, especially in dense solid mixtures. It is likely the lower kinetic energy barrier for which the $P4_3$ phase was synthesized regardless of the initial composition of CO–N_2 mixtures.

CO+Fe:[159] Potentially, advanced framework structures can be made by doping low-Z extended solids with functional transition metals. Organometallic compounds with weak metal-ligand bonds provide opportunities to synthesize functional extended solids. For example, the phase diagram of $Fe(CO)_5$ (Fig. 11) indicates a limited stability of molecular $Fe(CO)_5$ phases within a PT region below the liquid/phase II/polymer triple point. The limited stability, in turn, signifies the temperature-induced weakening of Fe–CO back bonds, which eventually leads to the dissociation of Fe–CO at the onset of CO polymerization. The recovered polymer is a composite of layered crystalline hematite Fe_2O_3[160] and amorphous carbon-oxygen polymers. These results, therefore, demonstrate the synthesis of carbon-oxygen polymer by compressing $Fe(CO)_5$, which provides a novel synthetic route to developing transition metals bearing high energy density solids by compressing organometallic compounds.

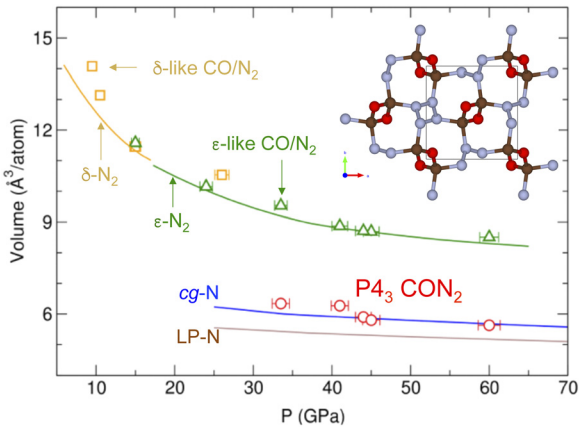

FIG. 10. Pressure-volume compression curves of extended (red circles) and molecular (green triangles and yellow squares) CON_2 phases in comparison with those of *cg*-N (blue line), LP-N (brown), δ-N_2 (yellow), and ε-N_2 (green). The inset shows the crystal structure of $P4_3$ solid, consisting of four-fold coordinated carbon atoms (brown), three-fold nitrogen (gray), and two-fold oxygen (red) in a three-dimensional framework structure [Reprinted with permission from C.-S. Yoo *et al.*, J. Phys. Chem. C **122**, 13054 (2018). Copyright (2017) American Chemical Society].

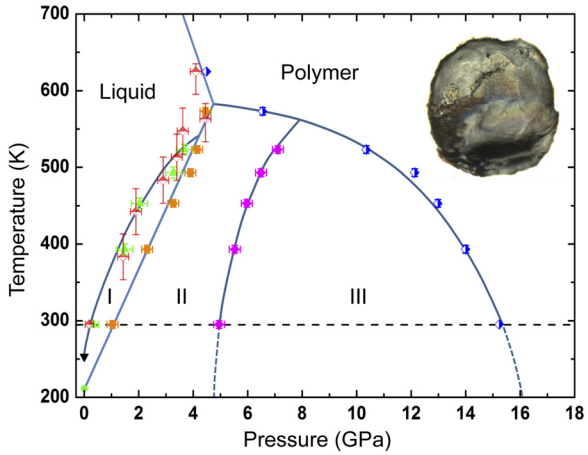

FIG. 11. Phase diagram of $Fe(CO)_5$, consisting of liquid, three molecular phases (noted as I, II, and III), and a polymeric product. Note that unreacted $Fe(CO)_5$ is stable within a limited pressure-temperature range, reflecting the weakness of Fe–CO back bonds with increasing temperatures. The inset shows the lustrous appearance of recovered $Fe(CO)_5$ polymer, coming from a graphite-like 2D carbon-oxygen polymer on the surface [Reprinted with permission from Y. J. Ryu *et al.*, Sci. Rep. **5**, 15139 (2015). Copyright 2015 Macmillan Publishers Ltd.].

Interest in 3*d* metal-doped low-Z extended solids centers on the goal of stabilizing highly metastable low-Z network structures by forming metal low-Z organic bonds, while harvesting the functional properties of 3*d* transition metals and unusual mechanical properties of *dense* metal-organic framework (*de*MOF) materials. The variety in electron polarity, structure, strength, and bond energy of metal-organic bonds, as well as the catalytic effect of metal species, can provide alternative reaction pathways to low-Z extended solids at more practically viable pressures and give rise to novel functional properties from doped metals, such as electric conductivity or magnetism.[151] Soft and more ionic metal atoms provide a flexibility to the rigid sp^2 and sp^3 covalent networks of low-Z extended solids, resulting in a unique combination of high-strength and ductility,[161] while the metastable nature of interfaces can facilitate the kinetic healing of damaged structures[162] and thereby enhanced stabilities. Polar atoms (N, O, H, F, and even C) of low-Z extended solids can directly bind metal ions by forming metal–low-Z bonds or entrap metal atoms in the interstitial sites of extended framework structures.[163,164] In such cases, the individual metal atoms or ions coupled to low-Z extended solids may introduce new magnetic, optical, and electric properties, arising from metal-organic hybridizations, charge transfers, electrostatic bindings, or van der Waals interactions.

X. CONCLUDING REMARKS

The recent discoveries of novel states and new materials under extreme conditions reveal several fundamental concepts governing the chemistry of dense solids under extreme conditions. These include the pressure evolution of chemical bonding and structure in dense

solids from molecular solids to covalent, ionic, and, ultimately, metallic solids, as well as the novel properties and complex transition mechanisms arising from the subtle balance between the electron hybridization (bonding) and electrostatic interaction (packing) in densely packed solids. We have emphasized that, while many of these transitions are predictive based on thermodynamic constraints, the mechanisms are rather complex and are often controlled by strong kinetics. Especially important are the kinetic controlled processes in the transition regions of structural miscibility at relatively low pressures, chemical bonding in an intermediate-pressure range, and electrostatic packing at extremely high pressures. A profound knowledge gap in both theory and experiment motivates future studies on the novel states, transformations, and chemical mechanisms of dense solids in these transition regions.

Modern advances in experimental and computational capabilities bring us closer to the goal of developing new materials on the basis of computational design coupled with experimental discovery and characterization. The application of large compression energies, comparable to chemical bond energies in solids, can advance the concept of materials by design in unique ways by converting molecular solids into novel 3D network structures that can be predicted on the basis of first principles and materials data-based computational science. This control and manipulation of chemical bonding is particularly effective in the case of solids made from low-Z elements, in which thermo-mechanical energies rapidly become substantially larger than those associated with the formation and diffusion of defects and grain boundaries. Importantly, these dense framework solids, when made of low-Z elements, are intrinsically hard yet light, e.g., diamond and c-BN, and exhibit superior thermal, mechanical, chemical, and electro-optical properties. Thus, they constitute the next generation of structural materials that are dense, light, multifunctional frameworks.

With modern advances in high-pressure and laser technologies, it is now possible to achieve the extreme PT conditions of the giant planets and the large compressions that force materials into fundamentally new physical and chemical configurations. Thus, the chemistry concepts presented in this paper have important implications with regard to the development of new planetary models, condensed materials theories, and extreme chemistries involving deep core electrons.

ACKNOWLEDGMENTS

The experimental results reported in this article have been performed previously in collaboration with Dr. Young-Jay Ryu, Dr. Minseob Kim, Dr. Dane Tomasino, Dr. Ranga Dias, Dr. Magnus Lipp, and Dr. William Evans. The author thanks Dr. John Tse for numerous scientific discussions and also Dr. Guouyin Shen and Dr. Jesse Smith at the HPCAT/APS, Peter Liermann at the PETRA-III, and Yasuo Oishi at the SPring-8 for their technical assistance.

The present study has been performed in support of the NSF (Grant No. DMR 1701360), DOE-NNSA (Grant No. DE-NA0003342), ARO (Grant No. W911NF-17-1-0468), DARPA (Grant No. W31P4Q-12-1-0009), and ADD in Korea.

REFERENCES

[1]D. S. Spiegel, J. J. Fortney, and C. Sotin, "Structure of exoplanets," Proc. Natl. Acad. Sci. U. S. A. **111**, 12622–12627 (2014).
[2]B. Buffett and D. Archer, "Global inventory of methane clathrate," Earth Planet. Sci. Lett. **227**, 185–199 (2004).
[3]C. S. Yoo and M. F. Nicol, "Chemical and physical transformation of cyanogen at high pressures," J. Phys. Chem. **90**, 6726–6731 (1986).
[4]K. Aoki, S. Usuba, M. Yoshida, Y. Kakudate, K. Tanaka, and S. Fujiwara, "Raman study of the solid-solid polymerization of acetylene at high pressure," J. Chem. Phys. **89**, 529–534 (1988).
[5]X. D. Wen, R. Hoffmann, and N. W. Ashcroft, "Benzene under high pressure: A story of molecular crystals transforming to saturated networks, with a possible intermediate metallic phase," J. Am. Chem. Soc. **133**, 9023–9025 (2011).
[6]F. P. Bundy, H. T. Hall, H. M. Strong, and R. H. Wentorf, "Man-made diamonds," Nature **176**, 51–55 (1955).
[7]C. Mailhiot, L. H. Yang, and A. K. McMahan, "Polymeric nitrogen," Phys. Rev. B **46**, 14419–14435 (1992).
[8]M. I. Eremets, A. G. Gavriliuk, I. A. Trojan, D. A. Dzivenko, and R. Boehler, "Single bonded cubic form of nitrogen," Nat. Mater. **3**, 558–563 (2004).
[9]M. J. Lipp, J. P. Klepeis, B. J. Baer, H. Cynn, W. J. Evans, V. Iota, and C. S. Yoo, "Transformation of molecular nitrogen to nonmolecular phases at megabar pressures by direct laser heating," Phys. Rev. B **76**, 014113 (2007).
[10]V. Iota, C. S. Yoo, and H. Cynn, "Quartzlike carbon dioxide: An optically nonlinear extended solid at high pressures and temperatures," Science **283**, 1510–1512 (1999).
[11]S. Serra, C. Cavazzoni, G. L. Chiarotti, S. Scandolo, and E. Tosatti, "Pressure-induced solid carbonates from molecular CO_2 by computer simulation," Science **284**, 788–790 (1999).
[12]C. S. Yoo, H. Cynn, F. Gygi, G. Galli, V. Iota, M. F. Nicol, S. Carlson, D. Hausermann, and C. Mailhiot, "Crystal structure of carbon dioxide at high pressure: "superhard" polymeric carbon dioxide," Phys. Rev. Lett. **83**, 5527–5530 (1999).
[13]F. Datchi, B. Mallick, A. Salamat, and S. Ninet, "Structure of polymeric carbon dioxide CO_2-V," Phys. Rev. Lett. **108**, 125701-1–125701-4 (2012).
[14]Ph. Pruzan, "Pressure effects on the hydrogen bond in ice up to 80," GPa **322**, 279–286 (1994).
[15]A. F. Goncharov, V. V. Struzhkin, M. S. Somayazulu, R. J. Hemley, and H. K. Mao, "Compression of ice to 210 gigapascales: Infrared evidence for a symmetric hydrogen-bonded phase," Science **273**, 218–220 (1996).
[16]P. Loubeyre, R. LeToullec, E. Wotanint, M. Hanfland, and D. Hausermann, "Modulated phases and proton centering in ice observed by x-ray diffraction up to 170 GPa," Nature **397**, 503–506 (1999).
[17]N. W. Ashcroft, "Metallic hydrogen: A high-temperature superconductor?," Phys. Rev. Lett. **21**, 1748–1749 (1968).
[18]M. I. Eremets and I. A. Troyan, "Conductive dense hydrogen," Nat. Mater. **10**, 927–931 (2011).
[19]R. P. Dias and I. F. Silvera, "Observation of the Wigner-Huntington transition to metallic hydrogen," Science **355**, 715–718 (2017).
[20]D. Ducan, Y. Liu, F. Tan, D. Li, X. Huang, Z. Zhao, H. Yu, B. Liu, W. Tian, and T. Cui, "Pressure-induced metallization of dense $(H_2S)_2H_2$ with high T_c superconductivity," Sci. Rep. **4**, 6968-1–6968-6 (2014).
[21]A. P. Drozdov, M. I. Eremets, I. A. Troyan, V. Ksenfontov, and S. I. Shylin, "Conventional superconductivity at 203 Kelvin at high pressures in the sulfur hydride system," Nature **525**, 73–76 (2015).
[22]C. J. Pickard and R. J. Needs, "Aluminium at terapascal pressures," Nat. Mater. **9**, 624–627 (2010).
[23]M.-S. Miao and R. Hoffmann, "High pressure electrides: A predictive chemical and physical theory," Acc. Chem. Res. **47**, 1311–1317 (2014).
[24]M.-S. Miao and R. Hoffmann, "High pressure electrides: The chemical nature of interstitial quasi-atoms," J. Am. Chem. Soc. **137**, 3631–3637 (2015).
[25]H.-K. Mao and R. J. Hemley, "The high-pressure dimension in earth and planetary science," Proc. Natl. Acad. Sci. U. S. A. **104**, 9114–9115 (2007).
[26]J. Hemley and N. W. Ashcroft, "The revealing role of pressure in the condensed matter," Phys. Today **51**(8), 26–32 (1998).
[27]R. Jeanloz, "Physical chemistry at ultrahigh pressures and temperatures," Ann. Rev. Phys. Chem. **40**, 237–259 (1989).
[28]C. J. Pickard and R. J. Needs, "High-pressure phases of silane," Phys. Rev. Lett. **97**, 045504-1–045504-4 (2006).

[29]L. Zhang, Y. Wang, J. Lv, and Y. Ma, "Materials discovery at high pressures," Nat. Rev. Mater. **2**, 17005 (2017).
[30]A. R. Oganov, A. O. Lyakhov, and M. Valle, "How evolutionary crystal structure prediction works-and why," Acc. Chem. Res. **44**, 227–237 (2011).
[31]Z. Zurek, R. Hoffmann, N. W. Ashcroft, A. R. Oganov, and A. O. Lyakhov, "A little bit of lithium does a lot for hydrogen," Proc. Natl. Acad. Sci. U. S. A. **196**, 17640–17643 (2009).
[32]C. S. Yoo, "New states of matter and chemistry at extreme pressures: Low-Z extended solid," MRS Bull. **42**, 724–728 (2017).
[33]C. S. Yoo, "Physical and chemical transformations of highly compressed carbon dioxide at bond energies," Phys. Chem. Chem. Phys. **15**, 7949–7966 (2013).
[34]Zs. Jenei, E. F. O'Bannon, S. T. Weir, H. Cynn, M. J. Lipp, and W. J. Evans, "Single crystal toroidal diamond anvils for high pressure experiments beyond 5 megabar," Nat. Commun. **9**, 3563-1–3563-6 (2018).
[35]A. Dewaele, P. Loubeyre, F. Occelli, O. Marie, and M. Mesouar, "Toroidal diamond anvil cell for detailed measurements under extreme static pressures," Nat. Commun. **9**, 2913-1–2913-9 (2018).
[36]N. Dubrovinskaia, L. Dubrovinsky, N. A. Solopova, A. Abakumom, S. Turner, M. Hanfland, E. Bykova, M. Bykov, C. Prescher, V. B. Prakapenka, S. Petitgirard, I. Chuvashova, B. Gasharova, Y.-L. Mathis, P. Ershov, I. Snigireva, and A. Sniglrev, "Terapascal static pressure generation with ultrahigh yield strength nanodiamond," Sci. Adv. **2**, e1600341-1–e1600341-12 (2016).
[37]M. J. Lipp, W. J. Evans, and C. S. Yoo, "Cryogenic loading of large volume presses for high-pressure experimentation and synthesis of novel materials," Rev. Sci. Instrum. **76**, 053903-1–053903-4 (2005).
[38]J. Xu and H.-K. Mao, "Moissanite: A window for high-pressure experiements," Science **290**, 783–785 (2000).
[39]Z. Wang, D. He, W. Zhang, W. Li, W. Li, J. Qin, L. Lei, Y. Zou, and X. Yang, "Portable high pressure sapphire anvil cell for gas hydrates research," Rev. Sci. Instrum. **81**, 085102-1–085102-5 (2010).
[40]S. N. Monteiro, A. L. D. Skury, M. G. de Azevedo, and G. S. Bobrovnitchii, "Cubic boron nitride competing with diamond as a superhard engineering materials—An overview," J. Mater. Res. Technol. **2**, 68–74 (2013).
[41]H. Sumiya, "Novel development of high-pressure synthetic diamonds "ultra-hard nano-polycrystalline diamonds"," SEI Technol. Rev. **74**, 15–22 (2012).
[42]G. W. Lee, W. J. Evans, and C.-S. Yoo, "Crystallization of water in a dynamic diamond-anvil cell: Evidence for ice VII-like local order in supercompressed water," Phys. Rev. B **74**, 134112-1–134112-6 (2006).
[43]G. W. Lee, W. J. Evans, and C. S. Yoo, "Dynamic pressure-induced dendrite and shock crystal growth of ice VI," Proc. Natl. Acad. Sci. U. S. A. **104**, 9178–9181 (2007).
[44]W. J. Evans, C. S. Yoo, G. W. Lee, H. Cynn, M. J. Lipp, and K. Visbeck, "Dynamic diamond anvil cell (d-DAC): A novel device for studying the dynamic-pressure properties of materials," Rev. Sci. Instrum. **78**, 073904-1–073904-6 (2007).
[45]J.-Y. Chen and C. S. Yoo, "Formation and phase transitions of methane hydrates under dynamic loadings: Compression rate dependent kinetics," J. Chem. Phys. **136**, 114513-1–114513-10 (2012).
[46]J.-Y. Chen, C.-S. Yoo, W. J. Evans, H.-P. Liermann, H. Cynn, M. Kim, and Z. Jenei, "Solidification and fcc- to metastable hcp- phase transition in krypton under variable compression rates," Phys. Rev. B **90**, 144104-1–144104-8 (2014).
[47]J. Y. Chen and C. S. Yoo, "High density amorphous ice at room temperature," Proc. Natl. Acad. Sci. U. S. A. **108**, 7685–7688 (2011).
[48]D. Tomasino and C. S. Yoo, "Solidification and crystal growth of highly compressed hydrogen and deuterium: Time-resolved study under ramp compression in dynamic-diamond anvil cell," Appl. Phys. Lett. **103**, 061905-1–061905-4 (2013).
[49]Y.-J. Kim, Y.-H. Lee, S. Lee, H. Nada, and G. W. Lee, "Shock growth of ice crytal near equilibrium melting pressure under dynamic compression," Proc. Natl. Acad. Sci. U. S. A. **116**, 8679–8684 (2019).
[50]J. K. Wicks, R. F. Smith, D. E. Fratanduono, F. Coppari, R. G. Kraus, M. G. Newman, R. J. Rygg, J. H. Eggert, and T. S. Duffy, "Crystal structure and equation of state of Fe-Si alloys at super-Earth core conditions," Sci. Adv. **4**, eaao5865-1–eaao5865-10 (2018).
[51]R. F. Smith, J. H. Eggert, R. Jeanloz, T. S. Duffy, D. G. Braun, J. R. Patterson, R. E. Rudd, J. Blener, A. E. Lazicji, A. V. Hamza, J. Wang, T. Braun, L. X. Benedict, P. M. Celliers, and G. W. Collins, "Ramp compression of diamond to five terapascals," Nature **511**, 330–333 (2014).
[52]P. M. Celliers, M. Millot, S. Brygoo, R. S. McWilliams, D. E. Fratanduono, J. R. Rygg, A. F. Goncharov, P. Loubeyre, J. H. Eggert, J. L. Peterson, N. B. Meezan, S. Le Pape, G. W. Collins, R. Jeanloz, and R. J. Hemley, "Insulator-metal transition in dense fluid deuterium," Science **361**, 677–682 (2018).
[53]A. L. Kritcher, T. Doppner, D. Swift, J. Hawreliak, G. Collins, J. Nilsen, B. Bachmann, E. Dewald, D. Strozzi, S. Felker, O. L. Landen, O. Jones, C. Thomas, J. Hammer, C. Keane, H. J. Lee, S. H. Glenzer, S. Rothman, D. Chapman, D. Kraus, P. Neumayer, and R. W. Falcone, "Probing matter at Gbar pressures at the NIF," High Energy Density Phys. **10**, 27–34 (2014).
[54]S. J. Turneaure, S. M. Sharma, T. J. Volz, J. M. Winey, and Y. M. Gupta, "Transformation of shock-compressed graphite to hexagonal diamond in nanoseconds," Sci. Adv. **3**, eaao3561-1–eaao3561-6 (2017).
[55]M. D. Knudsen, M. P. Desjarlais, A. Becker, R. W. Lemke, K. R. Cochrane, M. E. Savage, D. E. Bliss, T. M. Mattsson, and R. Redmer, "Direct observation of an abrupt insulator to metal transition in dense liquid deuterium," Science **348**, 1455–1460 (2015).
[56]S. T. Weir, A. C. Mitchell, and W. J. Nellis, "Metallization of fluid molecular hydrogen at 140 GPa (1.4 Mbar)," Phys. Rev. Lett. **76**, 1860–1864 (1996).
[57]S. M. Sharma, S. J. Turneaure, J. M. Winey, Y. Li, P. Rigg, A. Schuman, N. Sinclair, T. Toyoda, X. Wang, N. Weir, J. Zhang, and Y. M. Gupta, "Structural transformation and melting in gold shock compressed to 355 GPa," Phys. Rev. Lett. **123**, 045702-1–045702-4 (2019).
[58]R. L. Gustavsen, D. M. Dattelbaum, E. B. Watkins, M. A. Firestone, D. W. Podlesak, B. J. Jensen, B. S. Ringstrand, R. C. Huber, J. T. Mang, C. E. Johnson, K. A. Velizhanin, T. M. Wiley, D. W. Hansen, C. M. May, R. L. Hodgin, M. Bagge-Hansen, A. W. van Buuren, L. M. Lauderbach, A. C. Jones, T. J. Graber, N. Sinclair, S. Seifert, and T. Gog, "Time resolved small angle x-ray scattering experiments performed on detonating explosives at the advanced photon source: Calculation of the time and distance between the detonation front and the x-ray beam," J. Appl. Phys. **121**, 105902-1–105902-10 (2017).
[59]C. E. Wahrenberg, D. McGonegle, C. Bolme, A. Higginbotham, A. Lazicki, H. J. Lee, B. Nagler, H. S. Park, B. A. Remington, R. E. Rudd, M. Sliwa, M. Suggit, D. Swift, F. Tavella, L. Zepeda-Ruis, and J. S. Wark, "*In-situ* x-ray diffraction measurement of shock-wave-driven twinning and lattice dynamics," Nature **550**, 496–499 (2017).
[60]D. Kraus, J. Vorberger, A. Pak, N. J. Hartley, L. B. Fletcher, S. Frydrych, E. Galtier, E. J. Gamboa, D. O. Gericke, S. H. Glenzer, E. Granados, M. J. MacDonald, A. J. Mackinnon, E. E. McBride, I. Nam, P. Neumayer, M. Roth, A. M. Saunders, A. K. Schuster, P. Sun, T. van Driel, T. Doppner, and R. W. Falcone, "Formation of diamonds in laser-compressed hydrocarbons at planetary interior conditions," Nat. Astron. **1**, 606–611 (2017).
[61]D. J. Erskine and W. J. Nellis, "Shock-induced martensitic transformation of highly oriented graphite to diamond," J. Appl. Phys. **71**, 4882–4886 (1992).
[62]D. H. Dolan and Y. M. Gupta, "Nanosecond freezing of water under multiple shock wave compression: Optical transmission and imaging measurements," J. Chem. Phys. **8**, 9050–9057 (2004).
[63]O. Tschauner, S.-N. Luo, P. D. Asimow, and T. J. Ahrens, "Recovery of stishovite-structure at ambient conditions out of shock-generated amorphous silica," Am. Mineral. **91**, 1857–1862 (2006).
[64]A. J. Davidson, R. P. Dias, D. M. Dattelbaum, and C.-S. Yoo, ""Stubborn" triamiotrinitobenzene: Unusually high chemical stability of a molecular solid to 150 GPa," J. Chem. Phys. **135**, 174507-1–174507-5 (2011).
[65]C.-S. Yoo, J. J. Furrer, G. E. Duvall, S. F. Agnew, and B. I. Swanson, "Effects of dilution on the ultraviolet and visible absorptivity of CS_2 under static and shock compression," J. Phys. Chem. **91**, 6577–6578 (1987).
[66]C. S. Yoo and Y. M. Gupta, "Time-resolved absorption changes of thin CS_2 samples under shock compression: Electronic and chemical implications," J. Phys. Chem. **94**, 2857–2865 (1990).
[67]J. J. Dick and J. P. Ritchie, "Molecular mechanics modeling of shear and the crystal orientation dependence of the elastic precursor shock strength in pentaerythritol tetranitrate," J. Appl. Phys. **76**, 2726 (1994).
[68]J. Aidun, M. S. T. Bukowinski, and M. Ross, "Equation of state and metallization of CsI," Phys. Rev. B **29**, 2611–2621 (1984).

[69]H. K. Mao, Y. Wu, R. J. Hemley, L. C. Chen, J. F. Shu, and L. W. Finger, "X-ray diffraction to 302 gigapascals: High pressure crystal structure of cesium iodide," Science **246**, 649–651 (1989).
[70]K. A. Goettel, J. H. Eggert, and I. F. Silvera, "Optical evidence for the metallization of xenon at 132(5) GPa," Phys. Rev. Lett. **62**, 665–668 (1989).
[71]R. Reichlin, K. E. Brister, A. K. McMahan, M. Ross, S. Martin, Y. K. Vohra, and A. L. Ruoff, "Evidence for the insulator-metal transition in xenon from optical, x-ray, and band-structure studies to 170 GPa," Phys. Rev. Lett. **62**, 669–672 (1989).
[72]H. K. Mao, Y. Wu, R. J. Hemley, L. C. Chen, J. F. Shu, L. W. Finger, and D. E. Cox, "High-pressure phase transition and equation of state of CsI," Phys. Rev. Lett. **64**, 1749–1752 (1990).
[73]M. I. Eremets, K. Shimizu, T. C. Kobayashi, and K. Amaya, "Metallic CsI at pressures of up to 220 gigapascals," Science **281**, 1333–1335 (1998).
[74]Y. Xu, J. S. Tse, A. R. Oganov, T. Cui, H. Wang, Y. Ma, and G. Zou, "Superconducting high-pressure phase of cesium iodide," Phys. Rev. B **79**, 144110-1–144110-5 (2009).
[75]T. Yagi, W. Utsumi, M.-A. Yamakata, T. Kikegawa, and O. Shimomura, "High-pressure in-situ x-ray diffraction study of the phase transformation from graphite to hexagonal diamond at room temperature," Phys. Rev. B **46**, 6031–6039 (1992).
[76]A. F. Goncharov, I. N. Makarenko, and S. M. Stishov, "Graphite at pressure up to 55 GPa: Optical properties and Raman scattering-amorphous carbon?," Sov. Phys. JETP **69**, 380–381 (1989).
[77]C.-S. Yoo, A. Sengupta, and M. Kim, "Carbon dioxide carbonates in the Earth's mantle: Implications to the deep carbon cycle," Angew. Chem., Int. Ed. **50**, 11415–11418 (2011).
[78]C. S. Yoo and M. F. Nicol, "Kinetics of a pressure-induced polymerization reaction of cyanogen," J. Phys. Chem. **90**, 6732–6736 (1986).
[79]K. Aoki, B. J. Baer, H. Cynn, and M. F. Nicol, "High pressure Raman study of one-dimensional crystals of the very polar molecular hydrogen cyanide," Phys. Rev. B **42**, 4298–4303 (1990).
[80]A. Shinozaki, K. Mimura, and T. Nishida, "Decomposition and oligomerization of 2,3-naphthyridine under high-pressure and high-temperature conditions," Sci. Rep. **9**, 7335-1–7335-9 (2019).
[81]W. Crochala, R. Hoffmann, J. Feng, and N. W. Ashcroft, "The chemical imagination at work in *very* tight places," Angew. Chem., Int. Ed. **46**, 3620–3642 (2007).
[82]F. A. Cotton and G. Wilkinson, *Advanced Inorganic Chemistry*, 5th ed. (Wiley, New York, 1988).
[83]W. Utsumi and T. Yagi, "Light-transparent phase formed by room-temperature compression of graphite," Science **252**, 1542–1544 (1991).
[84]W. L. Mao, H.-K. Mao, P. J. Eng, T. P. Trainor, M. Newwille, C.-C. Kao, D. L. Heinz, J. Shu, Y. Meng, and R. J. Hemley, "Bonding changes in compressed superhard graphite," Science **302**, 425–427 (2003).
[85]Z. Zeng, L. Yang, Q. Zeng, H. Lou, H. Sheng, J. Wen, D. J. Miller, Y. Meng, W. Yang, W. L. Mao, and H.-K. Mao, "Synthesis of quenchable amorphous diamond," Nat. Commun. **18**, 322-1–322-7 (2017).
[86]M. I. Eremets, A. G. Gavriliuk, N. R. Serebryanaya, I. A. Trojan, D. A. Dzivenko, R. Boehler, H. K. Mao, and R. J. Hemley, "Structural transformation of molecular nitrogen to a single-bonded atomic state at high pressures," J. Chem. Phys. **121**, 11296–11300 (2004).
[87]F. P. Bundy, "Direct conversion of graphite to diamond in static pressure apparatus," J. Chem. Phys. **38**, 631–643 (1963).
[88]W. E. Streib, T. H. Jordan, and W. N. Lipscomb, "Singe-crystal x-ray diffraction study of β nitrogen," J. Chem. Phys. **37**, 2962–2965 (1962).
[89]X. Yong, H. Liu, M. Wi, Y. Yao, J. S. Tse, R. Dias, and C. S. Yoo, "Crystal structures and dynamical properties of dense CO_2," Proc. Natl. Acad. Sci. U. S. A. **113**, 11110–11115 (2016).
[90]A. Sengupta, M. Kim, and C. S. Yoo, "Polymerization of carbon dioxide: A chemistry view of molecular-to-nonmolecular phase transitions," J. Phys. Chem. C **116**, 2061–2067 (2012).
[91]R. P. Dias, C. S. Yoo, V. V. Struzhkin, M. Kim, T. Muramatsu, T. Matsuoka, Y. Ohishi, and S. Sinogelkin, "Superconductivity in highly disordered dense carbon disulfide," Proc. Natl. Acad. Sci. U. S. A. **110**, 11720–11724 (2013).
[92]R. P. Dias, C. S. Yoo, M. Kim, and J. S. Tse, "Insulator-metal transition of highly compressed carbon disulfide," Phys. Rev. B **84**, 144104-1–144104-6 (2011).
[93]M. J. Lipp, W. J. Evans, B. J. Baer, and C. S. Yoo, "High-energy-density extended CO solid," Nat. Mater. **4**, 211–215 (2005).
[94]M. L. Cohen, "Calculation of bulk moduli of diamond and zinc-blende solids," Phys. Rev. B **32**, 7988–7991 (1985).
[95]A. Y. Liu and M. L. Cohen, "Prediction of new low compressibility solids," Science **245**, 841–842 (1989).
[96]W. L. McMillan, "Transition temperature of strong-coupled superconductors," Phys. Rev. **167**, 331–344 (1968).
[97]D. T. Cromer, R. L. Mills, D. Schiferl, and L. A. Schwalbe, "The structure of N_2 at 49 kbar and 299 K," Acta Crystallogr. B **37**, 8–11 (1981).
[98]D. Schiferl, S. Buchsbaum, and R. L. Mills, "Phase transitions in nitrogen observed by Raman spectroscopy from 0.4 to 27.4 GPa at 15 K," J. Phys. Chem. **89**, 2324–2330 (1985).
[99]E. Gregoryanz, A. F. Goncharov, R. J. Hemley, H.-K. Mao, M. Somayazulu, and G. Shen, "Raman, infrared, and x-ray evidence for new phases of nitrogen at high pressures and temperatures," Phys. Rev. B **66**, 224108-1–224108-5 (2002).
[100]E. Gregoryanz, A. F. Goncharov, R. J. Hemley, and H.-K. Mao, "High-pressure amorphous nitrogen," Phys. Rev. B **64**, 052103-1–052103-4 (2001).
[101]C. J. Pickard, R. J. Needs, and R. J., "High-pressure phases of nitrogen," Phys. Rev. Lett. **102**, 125702-1–125702-4 (2009).
[102]D. Tomasino, Z. Jenei, W. Evans, and C.-S. Yoo, "Melting and phase transitions of nitrogen under high pressures and temperatures," J. Chem. Phys. **140**, 244510-1–244510-8 (2014).
[103]D. Tomasino, M. Kim, J. Smith, and C. S. Yoo, "Pressure-induced symmetry-lowering transition in dense nitrogen to layered polymeric nitrogen (LP-N) with colossal Raman intensity," Phys. Rev. Lett. **113**, 205502-1–205502-4 (2014).
[104]Y. Ma, A. R. Oganov, Z. Li, Y. Xie, and J. Kotakoski, "Novel high pressure structure of polymeric nitrogen," Phys. Rev. Lett. **102**, 065501-1–065501-4 (2009).
[105]Y. Cui, B. Li, H. He, W. Zhou, B. Chen, and G. Qjan, "Metal-organic frameworks as platforms for functional materials," Acc. Chem. Res. **49**, 483–493 (2016).
[106]D. Laniel, G. Geneste, G. Weck, M. Mezouar, and P. Loubeyre, "Hexagonal layered polymeric nitrogen phase synthesized near 250 GPa," Phys. Rev. Lett. **122**, 066001-1–066001-5 (2019).
[107]X. L. Wang, Y. C. Wang, M. S. Miao, X. Zhong, J. Lv, T. Cui, J. F. Li, L. Chen, C. J. Pickard, and Y. M. Ma, "Cagelike diamondoid nitrogen at high pressures," Phys. Rev. Lett. **109**, 175502-1–175502-4 (2012).
[108]Y.-J. Ryu, M. Kim, J. Lim, R. Dias, D. Klug, and C.-S. Yoo, "Dense carbon monoxide to 160 GPa: Stepwise polymerization to two-dimensional layered solid," J. Phys. Chem. C **120**, 27548–27554 (2016).
[109]A. I. Katz, D. Schiferl, and R. L. Mills, "New phases and chemical reactions in solid carbon monoxide under pressure," J. Phys. Chem. **88**, 3176–3179 (1984).
[110]M. Ceppatelli, A. Serdyukov, R. Bini, and H. Jodl, "Pressure induced reactivity of solid CO by FTRI studies," J. Phys. Chem. B **113**, 6652–6660 (2009).
[111]W. J. Evans, M. J. Lipp, C. S. Yoo, H. Cynn, J. L. Herberg, and R. S. Maxwell, "Pressure-induced polymerization of carbon monoxide: Disproportionation and synthesis of an energetic lactonic polymer," Chem. Mater. **18**, 2520–2531 (2006).
[112]M. Ceppatelli, M. Pagliali, R. Bini, and H. J. Jodl, "High-pressure photoinduced synthesis of polynitrogen in δ and ε-nitrogen crystals substitutionally doped with CO," J. Phys. Chem. C **119**, 130–140 (2015).
[113]J. Sun, D. D. Klug, C. J. Pickard, and R. J. Needs, "Controlling the bonding and bond gaps of solid carbon monoxide with pressure," Phys. Rev. Lett. **106**, 145502-1–145502-4 (2011).
[114]S. Bernard, G. L. Chiarotti, S. Scandolo, and A. Tosatti, "Decomposition and polymerization of solid carbon monoxide under pressure," Phys. Rev. Lett. **81**, 2092–2095 (1998).
[115]K. Xia, J. Sun, C. J. Pickard, D. D. Klug, and R. J. Needs, Phys. Rev. B **95**, 144102-1–144102-4 (2017).
[116]A. Hermann, N. W. Ashcroft, and R. Hoffmann, "High pressure ices," Proc. Natl. Acad. Sci. U. S. A. **109**, 745–750 (2012).
[117]Y. Wang, H. Liu, J. Lv, L. Zhu, H. Wang, and Y. Ma, "High pressure partially ionic phase of water ice," Nat. Commun. **2**, 563-1–563-5 (2011).
[118]P. Demontis, R. LeSar, and M. L. Klein, "New high-pressure phases of ice," Phys. Rev. Lett. **60**, 2284–2287 (1988).

[119]W. A. Bassett, T. Takehashi, H.-K. Mao, and J. S. Weaver, "Pressure-induced phase transformation in NaCl," J. Appl. Phys. **39**, 319–325 (1968).
[120]T. Sakai, E. Ohtani, N. Hirao, and Y. Ohishi, "Equation of state of the NaCl-B_2 phase up to 304 GPa," J. Appl. Phys. **109**, 084912-1–084912-6 (2011).
[121]X. Chen and Y. Ma, "High-pressure structures and metallization of sodium chloride," Eur. Phys. Lett. **100**, 026005 (2012).
[122]W. Grochala, "Atypical compounds of gases, which have been called 'noble'," Chem. Soc. Rev. **36**, 1632–1696 (2007).
[123]M. Kim, M. Debessai, and C. S. Yoo, "Two- and three-dimensional extended solids and metallization of compressed XeF_2," Nat. Chem. **2**, 784–788 (2010).
[124]E. Stavorou, Y. Yao, A. F. Goncharov, S. S. Lobanov, J. M. Zaug, H. Liu, E. Greenberg, and V. B. Prakapenka, "Synthesis of xenon and iron-nickel intermetallic compounds at Earth's core thermodynamic conditions," Phys. Rev. Lett. **120**, 096001-1–096001-4 (2018).
[125]S. Jiang, N. Holtgrewe, S. S. Lobanov, F. Su, M. F. Mahmood, R. S. McWilliams, and A. F. Goncharov, "Metallization and molecular dissociation of dense fluid nitrogen," Nat. Commun. **9**, 2624-1–2624-6 (2018).
[126]B. Boates and S. A. Bonev, "First-order liquid-liquid phase transition in compressed nitrogen," Phys. Rev. Lett. **102**, 015701-1–015701-4 (2009).
[127]M. Frost, J. B. Kim, E. E. McBride, J. R. Peterson, J. S. Smith, P. Sun, and S. H. Glenzer, "High-pressure melt curve and phase diagram of lithium," Phys. Rev. Lett. **123**, 065701-1–065701-4 (2019).
[128]M. Hanfland, K. Syassen, N. E. Christensen, and D. L. Novikov, "New high-pressure phases of lithium," Nature **408**, 174–178 (2000).
[129]Y. Ma, M. I. Eremets, A. R. Oganov, Y. Xie *et al.*, "Transparent dense sodium," Nature **458**, 182–185e (2009).
[130]C. Cavazzoni, G. L. Chiarotti, S. Scandolo, E. Tosatti, M. Bernascono, and M. Parrinello, "Superionic and metallic states of water and ammonia at giant planet conditions," Science **283**, 44–46 (1999).
[131]M. Millot, F. Coppari, J. R. Rygg, B. A. Correa, S. Hamel, D. C. Swift, and J. H. Eggert, "Nanosecond x-ray diffraction of shock-compressed superionic water ice," Nature **569**, 251–255 (2019).
[132]D. A. Young, *Phase Diagrams of the Elements* (University of California Press, 1991).
[133]C. S. Yoo, V. Iota, H. Cynn, M. F. Nicol, J.-H. Park, T. Le Bihan, and M. Mezouar, "Disproportionation and other transformations of N_2O at high pressures and temperatures to lower energy, denser phases," J. Phys. Chem. B **107**, 5922–5025 (2003).
[134]W. J. Nellis, A. C. Mitchell, F. H. Ree, M. Ross, N. C. Holmes, R. J. Trainor, and D. J. Erskine, "Equation of state of shock-compressed liquids: Carbon dioxide and air," J. Chem. Phys. **95**, 5268–5272 (1991).
[135]B. Boates, A. M. Teweldeberhan, and S. A. Bonev, "Stability of dense liquid carbon dioxide," Proc. Natl. Acad. Sci. U. S. A. **109**, 14808–14812 (2012).
[136]S. Scandolo, "Liquid-liquid phase transition in compressed hydrogen from first-principles simulations," Proc. Natl. Acad. Sci. U. S. A. **100**, 3051–0353 (2003).
[137]S. A. Bonev, E. Schwegler, T. Ogitsu, and G. Galli, "A quantum fluid of metallic hydrogen suggested by first-principles calculations," Nature **431**, 669–672 (2004).
[138]C. Liu, H. Gao, Y. Wang, R. J. Needs, C. J. Pickard, J. Sun, H.-T. Wang, and D. Xing, "Multiple superionic states in helium-water compounds," Nat. Phys. **15**, 1065 (2019).
[139]Z. Liu, J. Botana, A. Hermann, S. Valdez, E. Zurek, D. D. Yan, H. Q. Lin, and M. S. Miao, "Reactivity of He with ionic compounds under high pressure," Nat. Commun. **9**, 951-1–951-10 (2018).
[140]W. Lorenzen, B. Holst, and R. Redmer, "Demixing of hydrogen and helium at megabar pressures," Phys. Rev. Lett. **102**, 115701-1–115701-4 (2009).
[141]G. M. Borstad and C. S. Yoo, "H_2O and D_2 mixtures under pressure: Spectroscopy and proton exchange kinetics," J. Chem. Phys. **135**, 174508-1–174508-11 (2011).
[142]G. M. Borstad and C.-S. Yoo, "Hydrogen bonding induced proton exchange reactions in dense D_2-NH_3 and D_2-CH_4 mixtures," J. Chem. Phys. **140**, 044510-1–044510-15 (2014).
[143]M. Kim and C.-S. Yoo, "Highly repulsive interaction in novel inclusion D_2-N_2 compounds at high pressure: Raman and X-ray evidence," J. Chem. Phys. **134**, 044519-1–044519-5 (2011).
[144]D. K. Spaulding, G. Weck, P. Loubeyre, F. Daichi, P. Dumas, and M. Hanfland, "Pressure-induced chemistry in a nitrogen-hydrogen host-guest structure," Nat. Commun. **5**, 5739-1–5739-7 (2014).
[145]J. Lim and C.-S. Yoo, "Intercalation of solid hydrogen into graphite under pressure," Appl. Phys. Lett. **109**, 051905-1–051905-5 (2016).
[146]C. S. Yoo, M. Kim, W. Morgenroth, and P. Liermann, "Transformation and structure of silicatelike CO_2-V," Phys. Rev. B **87**, 214103-1–214103-9 (2013).
[147]I. Valentin, C.-S. Yoo, J. Klepeis, J. Zsolt, W. Evans, and H. Cynn, Nat. Mater. **6**, 34–37 (2007).
[148]A. Sengupta and C.-S. Yoo, "Coesite-like CO_2: An analog to SiO_2," Phys. Rev. B **82**, 012105-1–012105-4 (2010).
[149]Y. J. Ryu, C. S. Yoo, M. Kim, X. Yong, J. Tse, S. K. Lee, and E. J. Kim, "Hydrogen-doped polymeric carbon monoxide at high pressure," J. Phys. Chem. C **121**, 10078–10086 (2017).
[150]C.-S. Yoo, M. Kim, J. Lim, Y. J. Ryu, and I. G. Batyrev, "Copolymerization of CO and N_2 to extended CON_2 framework solid at high pressures," J. Phys. Chem. C **122**, 13054-13960 (2018).
[151]S. Duwal, Y.-J. Ryu, M. Kim, C.-S. Yoo, S. Bang, K. Kim, and N. H. Hur, "Transformation of hydrazinium azide to molecular N_8 at 40 GPa," J. Chem. Phys. **148**, 134310-1–134310-7 (2018).
[152]K. O. Christe, W. W. Wilson, J. A. Sheechy, and J. A. Boatz, "N_5^+: A novel homoleptic polynitrogen ion as a high energy density material," Angew. Chem., Int. Ed. **38**, 2004–2009 (2004).
[153]J. C. Crowhurst, J. M. Zaug, H. R. Radousky, B. A. Steele, A. C. Landrville, and I. A. Oleynik, "Ammonium azide under high pressure: A combined theoretical and experimental study," J. Phys. Chem. A **118**, 8695–8700 (2014).
[154]H. Gao and J. M. Shreeve, "Azole-based energetic salts," Chem. Rev. **111**, 7377–7436 (2011).
[155]Z. Raza, C. J. Pickard, C. Pinilla, and A. Marco Saitta, "High energy density mixed polymeric phase from carbon monoxide and nitrogen," Phys. Rev. Lett. **111**, 235501-1–235501-5 (2013).
[156]C. Zhu, Q. Li, Y. Zhou, M. S. Zhang, S. Zhang, and Q. Li, "Exploring high-pressure structure of N_2CO," J. Phys. Chem. C **118**, 27252–27257 (2014).
[157]B. A. Steele and I. I. Oleynik, "Ternary inorganic compounds containing carbon, nitrogen, and oxygen at high pressures," Inorg. Chem. **56**, 13321–13328 (2017).
[158]J. A. Ciezak-Jenkins, B. A. Steele, G. M. Borstad, and I. I. Oleynik, "Structural and spectroscopic studies of nitrogen-carbon monoxide mixtures: Photochemical response and observation of a novel phase," J. Chem. Phys. **146**, 184309-1–184309-9 (2017).
[159]Y. J. Ryu, M. Kim, and C.-S. Yoo, "Phase diagram and transformations of iron pentacarbonyl to nm layered hematite and carbon-oxygen polymer under pressure," Sci. Rep. **5**, 15139-1–15139-8 (2015).
[160]G. K. Rozenberg, L. S. Dubrovinsky, M. P. Pasternak, O. Naaman, T. Le Bihan, and R. Ahuja, "High-pressure structural studies of hematite Fe_2O_3," Phys. Rev. B **65**, 064112-1–064112-8 (2002).
[161]B. Tang, Q. An, and W. A. Goddard III, "Improved ductility of boron carbide by microalloying with boron suboxide," J. Phys. Chem. C **119**, 24649–24656 (2015).
[162]F. R. Kersey, D. M. Loveless, and S. L. Craig, "A hybrid polymer gel with controlled rates of cross-link rupture and self-repair," J. R. Soc. Interface **4**, 373–380 (2007).
[163]A. P. Cote, A. I. Benin, N. W. Ockwig, M. O'Keefe, A. J. Matzger, and O. M. Yaghi, "Porous, crystalline, covalent organic frameworks," Science **310**, 1166–1170 (2005).
[164]D. J. Tranchemontague, J. L. Mendoza-Cortes, M. O'Keeffe, and O. M. Yaghi, "Secondary building units, nets and bonding in the chemistry of metal-organic frameworks," Chem. Soc. Rev. **38**, 1257–1283 (2009).